Analysis of the quasi-static approximation for calculating potentials generated by neural stimulation

2008 J. Neural Eng. 5 44

(http://iopscience.iop.org/1741-2552/5/1/005)

J. Neural Eng. **5** (2008) 44–53 doi:10.1088/1741-2560/5/1/005

Analysis of the quasi-static approximation for calculating potentials generated by neural stimulation

Chad A Bossetti, Merrill J Birdno and Warren M Grill

Department of Biomedical Engineering, Duke University, Hudson Hall 136, Box 90281, Durham, NC, 27708-0281, USA

E-mail: warren.grill@duke.edu

Received 11 July 2007
Accepted for publication 27 November 2007
Published 17 December 2007
Online at stacks.iop.org/JNE/5/44

Abstract

In models of electrical stimulation of the nervous system, the electric potential is typically calculated using the quasi-static approximation. The quasi-static approximation allows Maxwell's equations to be simplified by ignoring capacitive, inductive and wave propagation contributions to the potential. While this simplification has been validated for bioelectric sources, its application to rapid stimulation pulses, which contain more high-frequency power, may not be appropriate. We compared the potentials calculated using the quasi-static approximation with those calculated from the exact solution to the inhomogeneous Helmholtz equation. The mean absolute errors between the two potential calculations were limited to 5–13% for pulse widths commonly used for neural stimulation (25 μs-1 ms). We also quantified the excitation properties of extracellular point source stimulation of a myelinated nerve fiber model using potentials calculated from each method. Deviations between the strength–duration curves for potentials calculated using the quasi-static ($\sigma = 0.105$ S m^{-1}) and Helmholtz approaches ranged from 3 to 16%, with the minimal error occurring for 100 μs pulses. Differences in the threshold–distance curves for the two calculations ranged from 0 to 9%, for the same value of quasi-static conductivity. A sensitivity analysis of the material parameters revealed that the potential was much more strongly dependent on the conductivity than on the permittivity. These results indicate that for commonly used stimulus pulse parameters, the exact solution for the potential can be approximated by quasi-static simplifications only for appropriate values of conductivity.

(Some figures in this article are in colour only in the electronic version)

List of symbols

α	Attenuation constant, Np m^{-1}
β	Phase constant, rad m^{-1}
ε_0	Free space permittivity, 8.854×10^{-12} F m^{-1}
ε_c	Complex relative permittivity
ε_r	Relative permittivity, Real $\{\varepsilon_c\}$
Φ	Extracellular potential, volts
γ	Propagation constant, m^{-1}
σ	Conductivity, S m^{-1}
ω	Angular frequency, rad s^{-1}
ζ	Impedance density, Ohm m

1. Introduction

Electrophysiological modeling studies are typically carried out under the assumption that the dielectric properties of the tissue and the nature of bioelectric sources allow for a quasi-static solution for the potential. The quasi-static approximation enables Maxwell's equations to be simplified by ignoring capacitive, inductive and wave propagation effects. The basis for applying these simplifications to living tissue was originally derived by Plonsey and Heppner (1967). Their analysis was limited to signals generated by excitable cells within the body, where the spectral content of the signal was

limited to frequencies below 1 kHz. They focused exclusively on applications where the activity of this tissue is recorded at the body surface (e.g. EEG, ECG, EMG). By contrast, neural stimulation models are distinct from recording models in two key ways. First, contemporary stimulators generate rapidly rising, short duration pulses (~100 μs), whose frequency content extends well beyond 1 kHz. Second, the concern is not only that the extracellular potential may be affected by the quasi-static assumption, but that the outcome of stimulation may also be affected. Neuronal excitation is a nonlinear function of the extracellular potentials, and differences in the spatiotemporal distribution of the potentials may affect stimulus efficacy. These issues have not been addressed by any previous examination of the quasi-static approximation. The purpose of our investigation was to use first principles to determine if this approximation significantly affects the extracellular potentials generated by electrical stimulation, and whether these changes altered stimulus efficacy.

Recent studies have provided evidence that tissue acts as a frequency filter and argue that the quasi-static assumption may not always be appropriate. Bedard *et al* (2004) modeled this filtering effect in EEGs and local field potentials using spatial profiles for the extracellular conductivity and permittivity. Stinstra and Peters (1998) also modeled the tissue as being inhomogeneous, but treated the material properties as being frequency dependent. Both these studies showed that realistic volume conductor models could possess frequency-filtering characteristics. However, because the modeled signal sources were biological, the spectral content of the signal was limited. In addition, these studies focused on recording neural behavior, rather than on trying to alter it. Thus, we gain no insight as to whether their findings apply to neural stimulation.

An investigation by Butson and McIntyre (2005) implies that the quasi-static approximation may lead to an overestimate of the volume of tissue activated by neural stimulation. Their model included electrode and tissue capacitances, and incorporated realistic stimulus pulses. However, this analysis did not consider the inductive and propagation effects present in Maxwell's equations (Plonsey and Heppner 1967). In addition, the tissue conductivity was fixed, and only a limited number of permittivities were considered. The dielectric properties of tissue can exhibit strong frequency dependence (Duck 1990, Geddes and Baker 1967, Pethig and Kell 1987, Foster and Schwan 1989, Gabriel *et al* 1996a, 1996b, 1996c), and the impact of this dependence on the potentials is unclear.

In this analysis, we considered the accuracy of the quasi-static approximation for a neural stimulation model using a first-principles approach. An analytical expression for the potential in an infinite, homogeneous, isotropic volume conductor using a point current source stimulus was derived from the inhomogeneous Helmholtz wave equation. Using a myelinated nerve fiber model, we demonstrate the similarity between the strength–duration and threshold–distance curves for potentials calculated using the quasi-static and Helmholtz approaches. We also demonstrate that the potential is much more sensitive to the choice of conductivity than to the inclusion of the full range of dielectric phenomena. For commonly used stimulus pulse parameters, the exact solution for the potential can be approximated by quasi-static simplifications only for appropriately selected values of conductivity.

2. Theory

We calculated the potentials generated by a point source electrode in an infinite, homogeneous, isotropic volume conductor using both the quasi-static approximation and the exact solution to the inhomogeneous Helmholtz equation. The conductivity, σ (S m^{-1}), represented the effective conductivity of the material, and encompassed both the static and alternating conductivities, (where the alternating conductivity is brought on by the rotation of dipoles). The permittivity, ε (F m^{-1}), represented the product of the relative permittivity, ε_r, and the free space permittivity, ε_0. We will also refer to the complex relative permittivity, which is classically represented by the following expression:

$$\varepsilon_c = \varepsilon_r - j\frac{\sigma}{\omega\varepsilon_0} \tag{1}$$

where ω is the angular frequency. The complex permittivity is obtained from this expression by multiplying by ε_0. The permeability, μ (H m^{-1}), was assumed to be that of free space.

2.1. Quasi-static potential

Under quasi-static conditions, the potential was derived through the integral solution to Poisson's equation. This exercise has been exhaustively documented (Plonsey and Barr 2000, Plonsey and Collin 1961, Johnk 1988, Balanis 1989), and is withheld for brevity. The result is

$$\Phi(R) = \frac{I}{4\pi\sigma R}. \tag{2}$$

Here, Φ is the potential, I is the stimulus intensity and R is the distance between the source and field points. The conductivity, σ, is a real constant, and is not frequency dependent. For all quasi-static simulations, the default conductivity was 0.105 S m^{-1}. As discussed below, both the potential and excitation thresholds are strongly dependent on σ, and the above value was selected to minimize error in the potential for 100 μs pulses.

2.2. Time harmonic potential

When the quasi-static assumption is relaxed, the inhomogeneous Helmholtz equation must be solved:

$$\nabla\Phi - \gamma^2\Phi = \frac{\nabla\cdot\mathbf{J}}{\mathbf{j}\omega(\varepsilon_0\varepsilon_c)} = \frac{\nabla\cdot\mathbf{J}}{\sigma + \mathbf{j}\omega\varepsilon}. \tag{3}$$

The derivation of this equation is presented in the appendix. Within the expression, $\mathbf{J}$ is the current density and γ is the complex propagation constant, defined as

$$\gamma = \alpha + \mathrm{j}\beta, \tag{4}$$

where

$$\alpha = \omega\sqrt{\mu\varepsilon}\left\{\frac{1}{2}\left[\sqrt{1+\left(\frac{\sigma}{\omega\varepsilon}\right)^2} - 1\right]\right\}^{\frac{1}{2}} \tag{5}$$

$$\beta = \omega\sqrt{\mu\varepsilon}\left\{\frac{1}{2}\left[\sqrt{1+\left(\frac{\sigma}{\omega\varepsilon}\right)^2}+1\right]\right\}^{\frac{1}{2}}. \tag{6}$$

Here α (np m^{-1}) represents the amplitude decay and β (radians m^{-1}) represents the sinusoidal phase shift. The solution to equation (3) is typically expressed as an integral and the analytical expression in spherical coordinates is (Balanis 1989, Johnk 1988)

$$\Phi(r) = \frac{1}{4\pi(\sigma + \mathrm{j}\omega\varepsilon)}\int_V \frac{\nabla\cdot\mathbf{J}\,\mathrm{e}^{-\gamma r}}{r}\,\mathrm{d}V. \tag{7}$$

Here, the volume integral is taken over all space. For a fixed distance, R, from the source, this integral can be rewritten as a surface integral using the divergence theorem. We can also express the source current density in terms of the stimulus, I, by assuming spherical symmetry. Making these modifications and including unit vectors for a spherical coordinate system, equation (7) becomes

$$\Phi(R) = \frac{1}{4\pi(\sigma + \mathrm{j}\omega\varepsilon)}\oint_S\left(\frac{1}{R}\right)\frac{I\,\mathrm{e}^{-\gamma R}}{4\pi R^2}\,\mathbf{a}_r\cdot\mathbf{a}_r R^2\sin\theta\,\mathrm{d}\theta\,\mathrm{d}\phi. \tag{8}$$

Analytical evaluation of this integral yields

$$\Phi(R) = \frac{I\,\mathrm{e}^{-\gamma R}}{4\pi(\sigma + \mathrm{j}\omega\varepsilon)R}. \tag{9}$$

This result assumes that the source is oscillatory at a single frequency, ω. In general, we would like to write an expression for the potential that reflects the broadband nature of the stimulus current. Thus, the stimulus is written as a complex exponential Fourier series:

$$I = \sum_{n=-\infty}^{\infty} X_n\,\mathrm{e}^{\mathrm{j}n\omega_0 t}, \tag{10}$$

and the expression for the potential becomes

$$\Phi(R) = \sum_{n=-\infty}^{\infty}\frac{X_n\,\mathrm{e}^{(\mathrm{j}n\omega_0 t-\gamma_n R)}}{4\pi(\sigma_n + \mathrm{j}n\omega_0\varepsilon_n)R}. \tag{11}$$

Note that the dielectric parameters in equation (11) have been indexed to indicate their frequency-dependence, as described in the following section. The constant, ω_0, is the repetition frequency for a periodic stimulus pulse train. Complex Fourier coefficients, X_n, can be calculated for a specific stimulus waveform.

2.3. *Frequency-dependent dielectric properties*

The dielectric properties of tissue are frequency dependent (Duck 1990, Gabriel *et al* 1996c, Pethig and Kell 1987, Foster and Schwan 1989). For a single polarization mechanism, the complex relative permittivity can be approximated by the Debye equation (Debye 1929):

$$\varepsilon_c(\omega) = \varepsilon_\infty + \frac{\varepsilon_S - \varepsilon_\infty}{1 + \mathrm{j}\omega\tau}. \tag{12}$$

Here, ε_∞ is the permittivity as $\omega\to\infty$, ε_S is the permittivity as $\omega\to 0$ and τ is the relaxation time constant.

However, in tissue there are several polarization mechanisms that result in multiple dispersions, including the

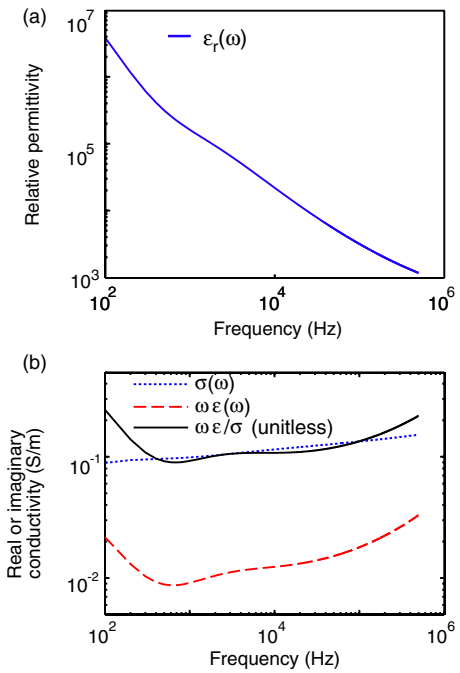

Figure 1. Frequency-dependent relative permittivity (ε_r) and conductivity (σ) of gray matter. The properties were based on a model developed by Gabriel *et al* (1996c). (a) The relative permittivity. (b) The real and imaginary components of conductivity. The ratio of the two components is also shown, for later comparison.

α, β, γ and δ dispersions, which are dominant at low, medium, high and very high frequencies, respectively (note that α and β, as used in this instance, do not indicate the components of the propagation constant). Each of the dispersions can be represented by a particular τ. Because these mechanisms interact, each dispersion region is broadened. Cole and Cole (1941) accounted for this effect by adding a distribution parameter to the Debye equation (12), resulting in the Cole–Cole equation:

$$\varepsilon_c(\omega) = \varepsilon_\infty + \frac{\varepsilon_S - \varepsilon_\infty}{1 + (\mathrm{j}\omega\tau)^{(1-\alpha)}}, \tag{13}$$

where α is the distribution parameter (not to be confused with either the type of dispersion or the attenuation constant). Gabriel *et al* (1996c) used multiple Cole–Cole dispersions to model the dielectric spectrum of various types of tissue:

$$\varepsilon_c(\omega) = \varepsilon_\infty + \sum_{n=1}^{4}\frac{\Delta\varepsilon_n}{1 + (\mathrm{j}\omega\tau_n)^{(1-\alpha_n)}} + \frac{\sigma_i}{\mathrm{j}\omega\varepsilon_0}. \tag{14}$$

Note that a static ionic conductivity term is included to account for the complete spectral behavior. In this expression, the $\Delta\varepsilon_n$ are the changes in relative permittivity as a result of each dispersion (α, β, γ and δ). It is also implicit in this equation that the real and imaginary terms can be equated with the corresponding terms in equation (1).

We used the parameters presented in Gabriel *et al* (1996c) for brain gray matter. The permittivity was then determined by multiplying the real part of equation (14) by ε_0, at the frequency of interest (figure 1(a)). Similarly, the frequency-dependent conductivity (figure 1(b)) was determined by multiplying the imaginary part of equation (14) by $\omega\varepsilon_0$.

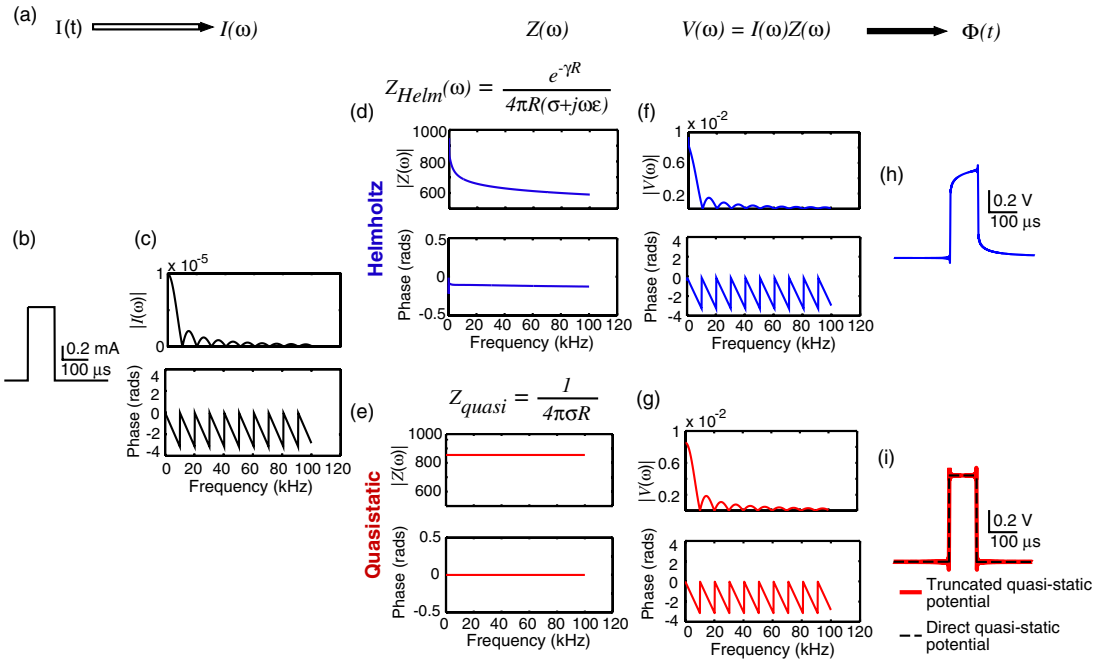

Figure 2. Comparison of potentials calculated from the Helmholtz solution and the quasi-static approximation of potentials. (a) Diagram of the four steps used to calculate the potentials. First, the periodic continuous time current pulse, $I(t)$, was represented as complex Fourier series coefficients $I(\omega)$ (open arrow). Second, the complex frequency-dependent impedances, $Z(\omega)$, were calculated for the Helmholtz and quasi-static approaches. Third, the frequency-dependent potentials, $V(\omega)$, were obtained by multiplying $I(\omega)$ and $Z(\omega)$. Fourth, $V(\omega)$ was multiplied by the complex time-dependent Fourier series term ($e^{jn\omega_0 t}$) and the product was summed over the length of the series for each time step (bold arrow), resulting in the potential as a function of time, $\Phi(t)$. (b) Time-domain current trace for a 1 mA cathodic pulse with a duration of 100 μs. (c) Amplitude and phase characteristics of $I(\omega)$. (d–e) Magnitude and phase characteristics of $Z(\omega)$ for the Helmholtz solution (d) and quasi-static approximation (e) ($R = 1$ mm). (f–g) Magnitude and phase characteristics of $V(\omega)$ for the Helmholtz solution (f) and quasi-static approximation (g). (h and i) The complete time domain Helmholtz (h) and quasi-static (i) representations of $\Phi(t)$ both demonstrated slight Gibbs phenomenon distortion and were quite similar. When the quasi-static potential was calculated directly, Gibbs phenomenon was eliminated; however, the potential was the same as the truncated quasi-static potential in all other respects. All magnitude and phase plots represent discrete Fourier series with $F_o = 100$ Hz and 5000 harmonics. Only frequency content up to 100 kHz is illustrated.

3. Methods

3.1. Stimulus waveforms

For all simulations, potentials were calculated from equation (11) using MATLAB (The Math Works, Natick, MA). The Fourier coefficients were determined for a square pulse, with a repetition frequency of 100 Hz. The series was truncated at 500 kHz, and to avoid aliasing, the sampling rate was 10 MHz (20 times the highest frequency component in the stimulus waveform). The waveforms were aligned such that each pulse began at $t = 500$ μs. To ensure a baseline potential of 0 V, a dc offset was subtracted from the time-shifted stimulus. This offset was determined by taking the mean of the potential from $t = 0$–20 μs.

3.2. Filtering properties of the Helmholtz solution

To compare and contrast the quasi-static and Helmholtz methods, we examined their frequency filtering properties in four steps (figure 2(a)). First, we computed the Fourier series of the periodic square wave stimulus current, and determined the amplitude and phase as a function of frequency, $I(\omega)$. Second, we calculated the frequency-dependent impedance used in the Helmholtz method, $Z_{\text{Helm}}(\omega)$:

$$Z_{\text{Helm}}(\omega) = \frac{e^{-\gamma R}}{4\pi(\sigma_\omega + j\omega\varepsilon_\omega)R}, \tag{15}$$

and the frequency-independent resistance used in the quasi-static method, Z_{quasi},

$$Z_{\text{quasi}} = \frac{1}{4\pi\sigma R} \tag{16}$$

where R represents the radial distance from the electrode. In the Helmholtz impedance, σ_ω and ε_ω were frequency dependent (figure 1); however, in the quasi-static case, σ was constant at 0.105 S m^{-1}. The third step was to multiply the frequency-dependent representations of the current, $I(\omega)$, and impedance, $Z(\omega)$, to yield a Fourier series representation of the potential, $V(\omega)$. Fourth, we calculated the time series potential, $\Phi(t)$, using equation (11). These quantities allowed us to compare the frequency filtering properties of the quasi-static and Helmholtz methods.

We quantified the percent error between the quasi-static estimate of the potentials, Φ_{quasi}, and Helmholtz solution of the potentials, Φ_{Helm}, at a given distance (R) and time (t) as follows:

$$\text{Error}_{\text{percent}} = 100\left|\frac{\Phi_{\text{quasi}}(R,t) - \Phi_{\text{Helm}}(R,t)}{\Phi_{\text{Helm}}(R,t)}\right|. \tag{17}$$

3.3. Neuronal excitation

We used a computer-based model of a myelinated nerve fiber to quantify differences in neuronal excitation by potentials calculated by the Helmholtz and quasi-static methods. The nerve fiber model consisted of a 20 μm diameter myelinated axon with 22 nodes. Each node contained leakage, fast sodium, persistent sodium and slow potassium currents (McIntyre and Grill 2000). Myelin internodes were 2 mm in length, and were electrically insulated from the extracellular space. Each node was 1.5 μm long, 12 μm in diameter and had a membrane capacitance of 2.5 μF cm^{-2}. All other nerve fiber parameters were taken from McIntyre and Grill (2000).

We used monophasic, cathodic, extracellular stimulation with a point source electrode to calculate strength–duration and threshold–distance curves. For strength–duration curve simulations, the electrode was positioned 1 mm above the center node of the axon and the stimulus pulse width was varied from 5 μs to 1 ms. Conversely, for threshold–distance curve simulations, the stimulus pulse width was held constant at 100 μs and the electrode-to-fiber distance was varied from 100 μm to 1 cm. At each electrode-to-fiber distance and stimulus pulse width, we varied the amplitude of the stimulus pulse until we identified the minimum current (threshold $\pm$ 0.2 μA) necessary to generate a propagating action potential in the nerve fiber. Individual simulations were run for a full period (10 ms) to determine whether a given stimulus pulse activated the model axon.

We also computed input–output curves for activation of a population of 100 identical parallel myelinated nerve fibers positioned randomly within a sphere of 3 mm radius. The stimulating point source electrode was positioned at the center of the sphere. The center node of each model fiber was positioned within the sphere by generating uniformly distributed random 3D coordinates. Each axon extended from the center node in both the positive and the negative x-directions, and the transmembrane potential was recorded at the end of each axon. Thresholds for each nerve fiber with a pulse width of 100 μs were calculated in the same manner as the strength–duration curves, and the percentage of nerve fibers stimulated as a function of stimulation amplitude was computed. Individual simulations were run for 5 ms—sufficient time to determine whether a given stimulus pulse activated the model axon. Potentials were only calculated for the 2 ms period beginning from -0.5 ms before the start of the pulse to 1.5 ms after the start of pulse, and were zero otherwise. This period was considered sufficient because approximately 99% of the decay to rest occurred within 1.5 ms after the beginning of these pulses.

Model nerve fiber simulations were implemented in NEURON (Hines and Carnevale 1997), and Crank–Nicholson integration was used to calculate the transmembrane potential in response to the extracellular stimulation with a time step of 1 μs (population model) or 0.1 μs (all other simulations).

4. Results

We compared the electrical potentials and resulting patterns of neuronal excitation calculated using both the quasi-static approximation and the exact solution to the inhomogeneous scalar Helmholtz equation.

4.1. Filtering properties of the Helmholtz solution

The filtering characteristics of the quasi-static and Helmholtz impedances, and the corresponding effects on the potential produced by a single stimulus pulse, are shown in figure 2. The stimulus, $I(t)$, had an amplitude of 1.0 mA, a pulse width of 100 μs and a repetition frequency of 100 Hz (figure 2(b)). The magnitude spectrum of the stimulus was a discretized sinc function, with envelopes spaced at 10 kHz intervals (figure 2(c)), and within each envelope, the phase decreased linearly from 0 to $-\pi$ (figure 2(c)).

While Z_{quasi} had no frequency-dependent characteristics, $Z_{\text{Helm}}(\omega)$ acted as a weak low-pass filter. This was evident in the magnitude of $Z_{\text{Helm}}(\omega)$, which decreased as a function of frequency (figure 2(d)). However, between 0 and 100 kHz, the magnitude of $Z_{\text{Helm}}(\omega)$ varied from the magnitude of Z_{quasi} by less than a factor of two (figures 2(d) and (e)), suggesting that the filtering was somewhat weak. The phase angles of the two impedances were also similar. The phase of Z_{quasi} was always zero, while the phase of $Z_{\text{Helm}}(\omega)$ only varied from -0.25 to 0 rad at very low frequencies and was constant at ~ -0.1 rad at higher frequencies (figures 2(d) and (e)).

When the frequency-dependent current and impedances were multiplied, the magnitudes and phases of the frequency-dependent quasi-static and Helmholtz potentials, $V(\omega)$, were nearly indistinguishable (figures 2(f) and (g)). The magnitudes of both potentials approximated discretized sinc functions with envelopes spaced at 10 kHz intervals (figures 2(f) and (g)). Within each envelope, the phase of the quasi-static potential decreased linearly from 0 to $-\pi$ rad (figure 2(g)), while the phase of the Helmholtz potential decreased linearly from 0 to -3.25 rad (figure 2(f))—varying only slightly from the quasi-static phase.

There were small but clear differences between time-domain versions of the Helmholtz and quasi-static potentials (figures 2(h) and (i)). As predicted by the magnitude of $Z_{\text{Helm}}(\omega)$, Φ_{Helm} appeared to be low-pass filtered with prolonged rise and fall times (figure 2(h)). Both Φ_{quasi} and Φ_{Helm} exhibited ringing at the onset and offset of the pulses as a result of truncating the Fourier series (figures 2(h) and (i)). For all simulations except those reported in figure 2, the Φ_{quasi} were calculated directly from equation (2). Nevertheless, by using the same Fourier series method to analyze both Φ_{quasi} and Φ_{Helm} in figure 2, we verified that the differences between Φ_{Helm} and Φ_{quasi} in subsequent analyses did not result from the Fourier representation of Φ_{Helm}.

4.2. Error analysis: quasi-static versus the Helmholtz solution

We calculated the errors between Φ_{quasi} and Φ_{Helm} for electrode-to-fiber distances ranging from 100 μm to 1 cm, and for pulse widths that varied from 5 μs to 1 ms. The percent error was not constant during a stimulus pulse, and the relative errors peaked at the beginning and end of the pulses, while the middle of the pulses was characterized by minimal errors

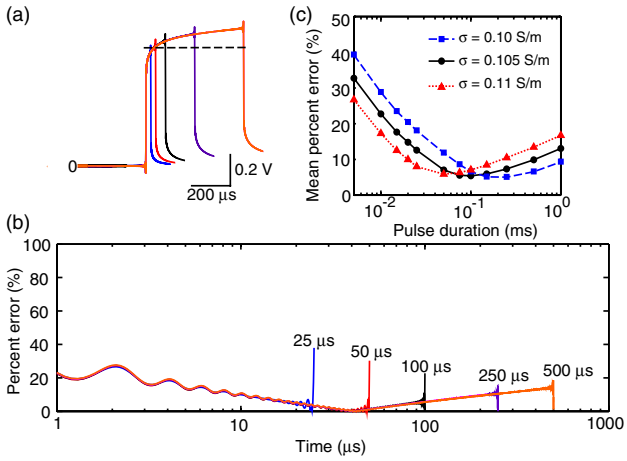

Figure 3. The percent error between the quasi-static estimate of the potentials, Φ_{quasi}, and Helmholtz solution of the potentials, Φ_{Helm}, was small across pulse widths commonly used in neural stimulation. (a) Sample traces of the potential as a function of time for five different pulse widths ($R = 1$ mm). The dashed line represents the magnitude of the quasi-static potential ($\sigma = 0.105$ S m^{-1}). After the pulse, the potentials calculated by the Helmholtz method decayed by 80% within a time equal to 3% of the pulse width. (b) The percent errors that were associated with the potentials shown in (a) evolved as a function of time ($R = 1$ mm, $\sigma = 0.105$ S m^{-1}). Note the log scale on the abscissa. The spikes in the error that occur at the end of a stimulus pulse reflect the rapid fall time in the quasi-static case. (c) percent error averaged over the duration of the quasi-static pulse for three estimates of quasi-static conductivity (0.105 S m^{-1}, 0.10 S m^{-1} and 0.11 S m^{-1}), with distance held constant at 1 mm. Changing the quasi-static conductivity estimate by approximately 5% shifted the minimum of the error curve along the pulse duration axis by approximately a factor of 2.

(figure 3(b)). To quantify the percent error associated with a given stimulus pulse, we averaged the percent errors over the duration of the quasi-static pulse (figure 3(c)). For pulse widths less than 25 μs, the mean percent errors ranged from 15 to 34%. However, the mean relative error was only 5–13% for pulse widths generally used for neural stimulation (25 μs to 1 ms), demonstrating that Φ_{quasi} provided a reasonable estimate of the extracellular potentials. We also varied the electrode-to-fiber separation from 10 μm to 1 cm, and with a 100 μs pulse, the relative error between the two potentials remained constant at 5.4%.

The pulse duration at which the minimum error occurred was strongly dependent on the conductivity. A ~5% change in σ resulted in a factor of two change in the pulse duration at which the minimum error occurred (figure 3(c)). In the following sections we provide further evidence that the conductivity is the most crucial material parameter for ensuring accuracy of the quasi-static approximation.

4.3. Sensitivity analysis

We conducted a sensitivity analysis to determine the effects of the parameters of the Helmholtz solution (γ, ε and σ) on the potential (equation (9)).

4.3.1. Propagation effects. To determine the effects of propagation due to the $e^{-\gamma R}$ term, we computed the magnitude

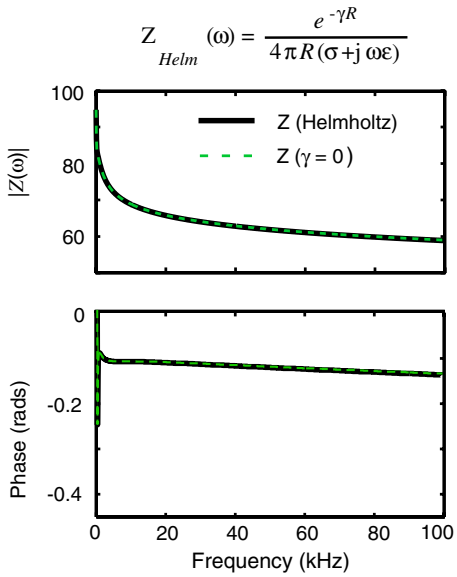

Figure 4. Propagation effects (from $e^{-\gamma R}$) were negligible. Magnitude and phase characteristics of $Z(\omega)$ are shown for the Helmholtz solution with and without including these effects ($R = R_{\text{max}} = 1$ cm). The magnitude and phase characteristics of $Z(\omega)$ were nearly identical for both cases. (Note that R is an order of magnitude larger than that used in figure 2(d).) Only frequency content up to 100 kHz is illustrated.

and phase of $Z_{\text{Helm}}(\omega)$ at a maximum distance of 1 cm from the electrode, both with and without propagation effects. When propagation was excluded, the magnitude and phase of $Z_{\text{Helm}}(\omega)$ did not change (figure 4); therefore, propagation effects can be neglected.

4.3.2. Sensitivity to conductivity and permittivity. To determine the effects of the permittivity and conductivity on the Helmholtz solution, we doubled and halved each parameter and examined the magnitude and phase of the radius-independent impedance density, $\zeta(\omega)$:

$$\zeta(\omega) = \frac{1}{(\sigma + j\omega\varepsilon)}. \tag{18}$$

When the conductivity was halved or doubled, both the magnitude and phase of ζ were doubled or halved (figure 5(a)). On the other hand, when the permittivity was halved or doubled, the phase of ζ was also halved or doubled, while the magnitude of ζ did not change (figure 5(a)).

The effects of changing the conductivity and permittivity were not limited to ζ; similar changes were observed in Φ_{Helm}. When the conductivity was halved or doubled, Φ_{Helm} was also halved or doubled (figure 5(b)). In contrast, when the permittivity was approximately halved or doubled, Φ_{Helm} changed by only 2–11% (figure 5(c)). These results indicate that Φ_{Helm} is more sensitive to changes in conductivity than changes in permittivity.

4.4. strength–duration and threshold–distance characteristics

We assessed the differences in neural excitation thresholds between Φ_{quasi} and Φ_{Helm}. Neuronal excitability was more

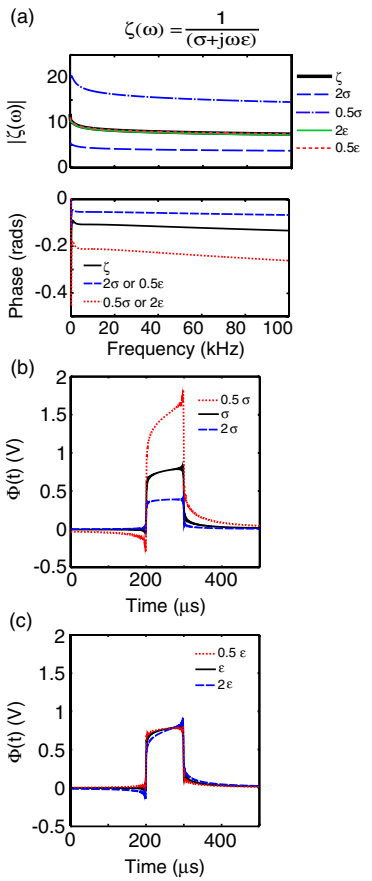

Figure 5. Potential was more strongly dependent on the conductivity than on the permittivity. (a) The magnitude and phase of the impedance density, $\zeta(\omega)$, are shown for baseline frequency-dependent dielectric properties, as well as for cases where either the conductivity or permittivity was doubled or halved, while the other was held constant. The magnitude was sensitive to changes in conductivity, but not changes in permittivity. In contrast, the phase was equally sensitive to changes in conductivity and permittivity. Only frequency content up to 100 kHz is illustrated. (b) The potential as a function of time for normal, halved and doubled conductivity. (c) The potential as a function of time for normal, halved and doubled permittivity. The potential was much more sensitive to changes in the conductivity than to changes in the permittivity. PW = 100 μs for (a–c), $R = 1$ mm for (b) and (c).

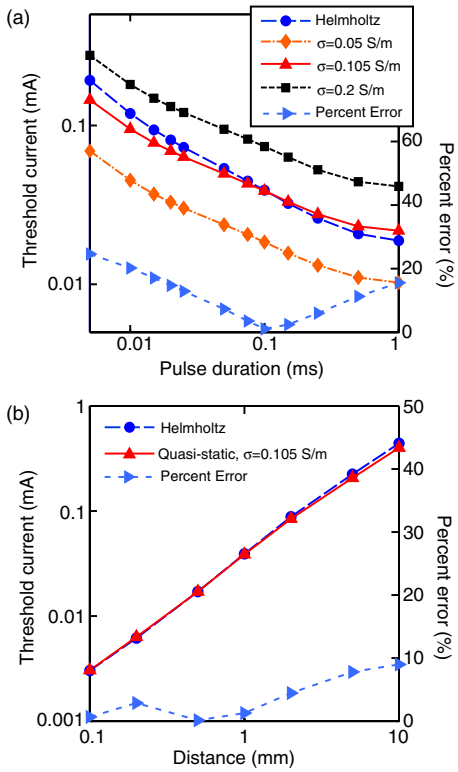

Figure 6. Neuronal excitability was similar for quasi-static estimates and Helmholtz solutions for the potential. (a) strength–duration curves are shown for an axon 1 mm from the point source electrode. Extracellular potentials were calculated from the Helmholtz solution and the quasi-static approximation with three different conductivities (0.05 S m^{-1}, 0.105 S m^{-1} and 0.2 S m^{-1}). (b) threshold–distance curves for a stimulus pulse width of 100 μs. For the Helmholtz solution, potentials were calculated over a full period (10 ms), starting from 0.5 ms before the beginning of the pulse and ending 9.5 ms after the beginning of the pulse. Note that the distance, pulse duration and threshold current axes are scaled logarithmically, while the percent error axis is scaled linearly.

strongly dependent on the conductivity than on carrying out the full Helmholtz solution. When the myelinated axon was stimulated by Φ_{quasi} calculated with the baseline conductivity ($\sigma = 0.105$ S m^{-1}), the strength–duration curves (figure 6(a)) and threshold–distance curves (figure 6(b)) were very similar to those calculated with Φ_{Helm}. The percent error between the threshold current calculated with Φ_{quasi} ($\sigma = 0.105$ S m^{-1}) and the threshold current calculated with Φ_{Helm} ranged from 3 to 16% (figures 6(a) and (b)) for pulse durations ranging from 25 μs to 1 ms (electrode-to-fiber distance = 1 mm), and across distances from 100 μm to 1 cm (pulse width = 100 μs). However, when the conductivity used to calculate Φ_{quasi} was halved or doubled, the thresholds for neuronal excitation were approximately halved or doubled (figure 6(a)). These results provide evidence that the excitation thresholds were more sensitive to the value of conductivity than to whether the potential was calculated with the quasi-static assumption or the full Helmholtz solution.

4.5. Input–output characteristics

We assessed the differences in neural recruitment between Φ_{quasi} and Φ_{Helm}. Input–output curves calculated with Φ_{quasi} and the baseline conductivity ($\sigma = 0.105$ S m^{-1}) were very similar to those calculated with Φ_{Helm} (figure 7). Similar to the case of a single fiber, the excitation of a population of neurons was strongly dependent on the conductivity. When the conductivity was halved or doubled, the amount of current required to excite a particular percentage of the fibers was also approximately halved and doubled, respectively.

5. Discussion

The objective of this study was to determine whether the quasi-static approximation is appropriate for calculating the potentials in models of extracellular stimulation of

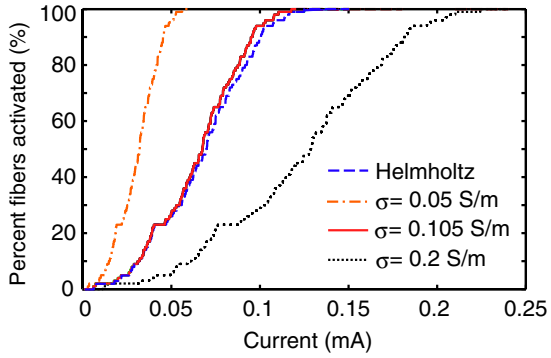

Figure 7. Input–output properties of a population of 100 randomly positioned axons activated by extracellular stimulation, with potentials calculated by Helmholtz and quasi-static methods. Three conductivity estimates were used for the quasi-static approximation (0.05 S m^{-1}, 0.105 S m^{-1} and 0.2 S m^{-1}).

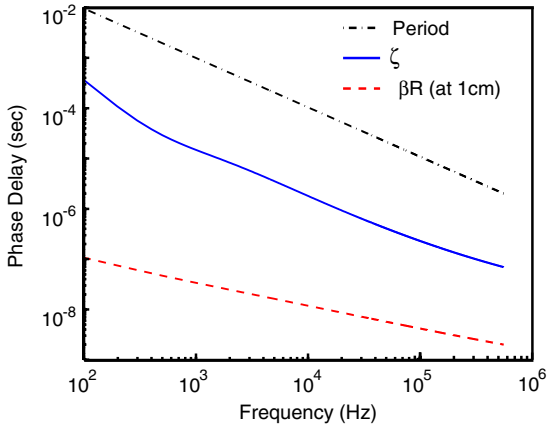

Figure 8. Phase delay resulting from impedance density and propagation effects. The impedance density results in a much larger phase delay than that from the propagation term, but is still more than an order of magnitude smaller than the period of each frequency that makes up the stimulus pulse.

neurons. In contrast to previous analysis that only considered low frequency biopotentials (Plonsey and Heppner 1967), this analysis considered the wide-band nature of potentials generated by rapid stimulating pulses, as well as the effects of the potentials on neuronal excitation. The quasi-static approximation is valid for pulse widths typically used for neural stimulation ($\sim$100 μs) when the value of conductivity is selected appropriately ($\sim$0.105 S m^{-1} for gray matter). The quasi-static approximation may lead to substantial errors depending on the duration (frequency content) of the stimulus pulse and on the value of the modeled conductivity (figure 6). To understand why the quasi-static approximation is valid for the particular conditions analyzed here, some discussion of the loss terms in equation (9) is required.

5.1. Loss due to damping and phase delay

There are two components that contribute to loss in traveling waves: damping and phase delay. For the potential described by equation (9), damping is caused by the α component of the propagation constant (γ, equation (4)) and by the factor R in the denominator. For the frequencies considered here, α ranges from 10^{-3} to 10^{-1} Np m^{-1}. Because distances are limited to $\leqslant$1 cm, the range of attenuation resulting from exponential damping is only 0.998–0.999. Thus, as demonstrated in figure 4, this term is not significant. On the other hand, the damping that results from the $1/R$ term is substantial. This factor changes the potential by an order of magnitude for an order of magnitude change in R.

The other component of loss, phase delay, also contributes little to the potentials. The solution to the Helmholtz equation introduces two sources of phase delay. The first is the βR component of the propagation constant; the other is the phase angle of ζ, the impedance density (equation (18)). The delay contributed by the propagation constant is shorter than the period of any of the sinusoids that make up the stimulus pulse by more than three orders of magnitude (figure 8). Additionally, the delay contributed by ζ is shorter than the period of any of the sinusoids by more than one order of magnitude, and for most frequencies, it is shorter by nearly two orders of magnitude. For the delay to have a major effect, the phase of each sinusoid would have to be shifted enough that the stimulus pulse is disrupted through destructive interference. For the relevant frequencies, the delay is limited to only 1/10 to 1/100 of the period, which is not sufficient to substantially disrupt the resulting potential.

Considering the effects of both α and β, it is clear that, for physiologic distances, the propagation effects represented by the $e^{-\gamma R}$ term in equation (9) can be ignored. A similar result is obtained for the $j\omega\varepsilon$ term in ζ (equation (18)), with a note of caution. The $j\omega\varepsilon$ component, which represents capacitive effects, is responsible for the qualitative changes in stimulus pulse morphology (figure 2(h)). The impact of this term on the potential will depend strongly on the frequency content of the stimulus pulse and the specific dielectric properties of the tissue. For the model of gray matter used in this study, σ is the dominant term in ζ (figure 1(b)), and both ζ and $\Phi(t)$ are much more dependent on σ than on ε (figures 6 and 7).

5.2. Comparison with classic quasi-static criteria

The bases for the quasi-static assumption were summarized in Plonsey and Heppner (1967). Several criteria were given for determining whether the propagation, inductive and capacitive effects could be ignored in Maxwell's equations. Here, we compare our findings with these criteria.

As stated above, the propagation effect is represented by the $e^{-\gamma R}$ term in equation (9). This effect is considered negligible if $|\gamma R| \ll 1$. In the present study, γ is frequency dependent; however, worst-case parameter values provide an upper bound. With $\alpha = 0.1$ Np m^{-1}, $\beta = 0.25$ rad m^{-1} and $R =$ 0.01 m, we have $|\gamma R| = 0.0027$ rad. Thus, our finding that propagation effects can be ignored is in agreement with this criterion.

If inductive effects are ignored, the Helmholtz equation (equation (3)) can be simplified to Poisson's equation, by ignoring the $j\omega A$ term in the expression for $\mathbf{E}$ (equation (A.1)). Inductive effects are negligible if $|\gamma R|^2 \ll 1$. So as long as the propagation effect is negligible (i.e. $|\gamma R| \ll 1$), then the inductive effect can also be ignored.

If capacitive effects are ignored, the medium is considered purely resistive and the $j\omega\varepsilon$ term in the denominator of equations (3) and (9) can be neglected. This simplification can be made if $\omega\varepsilon/\sigma \ll 1$, which states that the capacitive current must be much smaller than the conductive current. Again, these parameters are frequency dependent, but can be bounded. The ratio ranges from 0.24 at 100 Hz to 0.09 at 600 Hz. Across the spectrum (100 Hz to 500 kHz), the mean value of the ratio is approximately 0.17 (figure 1(b)). According to Plonsey and Heppner (1967), the criterion is fairly well satisfied for this range of values. Our finding that Φ_{quasi} differs from Φ_{Helm} by less than 13% leads us to conclude that the capacitive term can be ignored, under the conditions used in this study. However, of the three mathematical simplifications that make up the quasi-static approximation, elimination of the capacitive effects is the most questionable. The frequency content of the stimulus pulse and dielectric properties of the tissue must be considered before making this simplification.

5.3. Limitations

Several limitations of our computational approach require discussion. First, we approximated the stimulating electrode as a point source. For distances $\geqslant$50 μm from the electrode tip, a finely tipped microelectrode can be well approximated by a point source (McIntyre and Grill 2001). We examined the potentials at distances $\geqslant$100 μm from the source. While it is true that a given type of electrode may not lend itself to this approximation, the purpose of our study was to address the errors associated with the quasi-static assumption, not electrode geometry.

We used a model of dielectric tissue properties based on Gabriel *et al* (1996c), which itself may have several limitations. First, as a result of the impedance of the measurement electrodes, the measurements on which the model was based may contain errors at frequencies less than 1 kHz and substantial errors at frequencies less than $\sim$100 Hz (Gabriel *et al* 1996b). The authors indicate that these errors may affect the permittivity by a factor of two or three. However, our results showed that the potential is relatively unaffected by changes in ε. Second, this model does not incorporate tissue inhomogeneities. However, over the distances considered, it is reasonable to assume that the material is homogeneous. Finally, the model does not include anisotropy. Since the conductivity has a significant effect on the potential, and conduction can vary greatly between the longitudinal and transverse directions in a group of parallel fibers, care should be taken when applying the results of this study to tissue with a preferred orientation.

Another limitation was that a truncated Fourier series was used to approximate the square wave stimulus. Gibbs phenomenon was apparent in the time-domain potential solutions (figure 2), and the magnitude of the overshoot was approximately 9% of the stimulus magnitude. Even though these artifacts may not be representative of physical stimuli, our stimulus pulses exhibited 0.9 μs rise times, which is typical for commercially available stimulators. In addition, most of the power in this signal was located at frequencies below 10 kHz, and including frequencies as high as 500 kHz allowed us to represent accurately the power spectral density of the square wave stimulus.

Finally, there are several clinical features that were not accounted for in our model. For example, clinical stimulators typically apply charge-balanced, biphasic pulses, rather than monophasic pulses. However, complex pulse shapes can easily be implemented with our approach, through the use of the Fourier series. It is also well established that significant capacitance exists at the electrode–tissue interface. Again, such a feature could be incorporated for a more complete model. Our objective, though, was to study the validity of a common mathematical assumption used in stimulation models, rather than to investigate the effects of these clinical features.

6. Conclusion

The quasi-static approximation is a widely used simplification in electrophysiological modeling studies. To date, the validity of this simplification has not been thoroughly analyzed for neural stimulation, where the frequency content of a stimulus pulse extends well beyond that of bioelectric sources. We used the Helmholtz wave equation to determine the exact solution for the potential developed by a point source of current in a homogeneous isotropic medium. Within this model, we incorporated frequency-dependent dielectric properties, to account for tissue filtering characteristics. We then compared the resulting potential with that calculated using the quasi-static approximation. Because neural excitability is a nonlinear function of the extracellular potentials, we also compared the efficacy of stimulation of the two methods. We found that the errors between Φ_{quasi} and Φ_{Helm} were 5–13%, the errors in strength–duration curves were 3–16%, and the errors in threshold–distance curves were 0–9% for pulse widths from 25 μs–1 ms. These results highlight the similarity between the errors in the potentials and the errors in neuronal excitation.

These findings lead us to conclude that the quasi-static approximation is valid only over a limited range of conductivity. The phase delay and damping that result from propagation effects are completely negligible over physiologically relevant distances. Using the classic quasi-static criterion, the Helmholtz wave equation can be simplified to Poisson's equation, since inductive effects are also negligible. The most questionable simplification is whether the capacitive term can be neglected. Under the conditions established in our model, the capacitive term could be ignored, since the errors associated with its absence were limited to 16%. In general, before neglecting tissue capacitance, the criterion given in the section 5.2 should be consulted. Ultimately, the most important dielectric property is the conductivity. We estimate that for gray matter, choosing

$\sigma = 0.105$ S m^{-1} results in a neural response that is similar to that of the exact solution.

Acknowledgments

This work was supported by NIH grant R01 NS040894, a graduate research fellowship from the National Science Foundation and DARPA contract N66001-02-C-8022. The authors would also like to thank Dr S Nagarajan for his comments on the vector potential.

Appendix: Derivation of the inhomogeneous scalar Helmholtz equation

In this appendix, the expression for the inhomogeneous scalar Helmholtz equation is derived. We start from the expression for the electric field ($\mathbf{E}$), in terms of the vector potential ($\mathbf{A}$) and scalar potential (Φ).

$$\mathbf{E} = -\mathrm{j}\omega\mathbf{A} - \nabla\Phi. \tag{A.1}$$

Taking the divergence of both sides yields

$$\begin{aligned}\nabla\cdot\mathbf{E} &= \nabla\cdot(-\mathrm{j}\omega\mathbf{A} - \nabla\Phi)\\ &= -\mathrm{j}\omega(\nabla\cdot\mathbf{A}) - \nabla^2\Phi.\end{aligned} \tag{A.2}$$

According to the Helmholtz theorem, a vector is uniquely defined if its curl and divergence are specified. The curl of $\mathbf{A}$ is established by its definition ($\mathbf{B} = \nabla\times\mathbf{A}$). We are at liberty to choose its divergence. A typical assumption, which is appropriate in this case, is the *Lorentz condition* (or *gauge*):

$$\nabla\cdot\mathbf{A} = -\mathrm{j}\omega\varepsilon\mu\Phi. \tag{A.3}$$

Here, ω is the angular frequency, ε is the permittivity and μ is the permeability. Substituting this selection into equation (A.2) and simplifying yield

$$\nabla\cdot\mathbf{E} = -\omega^2\mu\varepsilon\Phi - \nabla^2\Phi. \tag{A.4}$$

Using the differential form of Gauss' law,

$$\nabla\cdot\mathbf{E} = \frac{\rho}{\varepsilon}, \tag{A.5}$$

we can rewrite equation (A.4)

$$\nabla^2\Phi + \omega^2\mu\varepsilon\Phi = -\frac{\rho}{\varepsilon}. \tag{A.6}$$

However, we would like to represent the scalar potential in terms of the stimulus current density, $\mathbf{J}$, rather than the charge density, ρ. Therefore, we employ the time-harmonic form of the law of conservation of charge,

$$\nabla\cdot\mathbf{J} = -\mathrm{j}\omega\rho. \tag{A.7}$$

Substituting this relation into equation (A.6)

$$\nabla^2\Phi + \omega^2\mu\varepsilon\Phi = \frac{\nabla\cdot\mathbf{J}}{\mathrm{j}\omega\varepsilon}. \tag{A.8}$$

This result represents the case of a lossless material. For a lossy dielectric, the permittivity must be replaced by the complex permittivity, as described in the section 2 (equation (1)).

$$\nabla^2\Phi + \omega^2\mu\left(\varepsilon - \mathrm{j}\frac{\sigma}{\omega}\right)\Phi = \frac{\nabla\cdot\mathbf{J}}{\mathbf{j}\omega\left(\varepsilon - \mathrm{j}\frac{\sigma}{\omega}\right)}. \tag{A.9}$$

Simplifying and rearranging the terms

$$\nabla^2\Phi - [\mathrm{j}\omega\mu\sigma - \omega^2\mu\varepsilon]\Phi = \frac{\nabla\cdot\mathbf{J}}{\sigma + \mathrm{j}\omega\varepsilon}. \tag{A.10}$$

The portion in brackets is referred to as γ^2. Thus, the final result is

$$\nabla^2\Phi - \gamma^2\Phi = \frac{\nabla\cdot\mathbf{J}}{\sigma + \mathrm{j}\omega\varepsilon}. \tag{A.11}$$

Note that this representation of γ^2 agrees with the nomenclature used in Plonsey and Heppner (1967), except for a minus sign. This choice will not affect the solution to the Helmholtz equation, in which the sign of the exponent is chosen to match physical conditions.

References

Balanis C A 1989 *Advanced Engineering Electromagnetics* (New York: Wiley)

Bedard C, Kroger H and Destexhe A 2004 Modeling extracellular field potentials and the frequency-filtering properties of extracellular space *Biophys. J.* **86** 1829–42

Butson C R and Mcintyre C C 2005 Tissue and electrode capacitance reduce neural activation volumes during deep brain stimulation *Clin. Neurophysiol.* **116** 2490–500

Cole K S and Cole R H 1941 Dispersion and absorption in dielectrics: I. Alternating current characteristics *J. Chem. Phys.* **9** 341–51

Debye P 1929 *Polar Molecules* (New York: The Chemical Catalog Company)

Duck F A 1990 *Physical Properties of Tissue: a Comprehensive Reference Book* (San Diego, CA: Academic Press)

Foster K R and Schwan H P 1989 Dielectric properties of tissues and biological materials: a critical review *Crit. Rev. Biomed. Eng.* **17** 25–104

Gabriel C, Gabriel S and Corthout E 1996a The dielectric properties of biological tissues: I. Literature survey *Phys. Med. Biol.* **41** 2231–49

Gabriel S, Lau R W and Gabriel C 1996b The dielectric properties of biological tissues: II. Measurements in the frequency range 10 Hz to 20 GHz *Phys. Med. Biol.* **41** 2251–69

Gabriel S, Lau R W and Gabriel C 1996c The dielectric properties of biological tissues: III. Parametric models for the dielectric spectrum of tissues *Phys. Med. Biol.* **41** 2271–93

Geddes L A and Baker L E 1967 The specific resistance of biological material—a compendium of data for the biomedical engineer and physiologist *Med. Biol. Eng.* **5** 271–93

Hines M L and Carnevale N T 1997 The NEURON simulation environment *Neural. Comput.* **9** 1179–209

Johnk C T A 1988 *Engineering Electromagnetic Fields and Waves* (New York: Wiley)

Mcintyre C C and Grill W M 2000 Selective microstimulation of central nervous system neurons *Ann. Biomed. Eng.* **28** 219–33

Mcintyre C C and Grill W M 2001 Finite element analysis of the current-density and electric field generated by metal microelectrodes *Ann. Biomed. Eng.* **29** 227–35

Pethig R and Kell D B 1987 The passive electrical properties of biological systems: their significance in physiology, biophysics and biotechnology *Phys. Med. Biol.* **32** 933–70

Plonsey R and Barr R C 2000 *Bioelectricity: A Quantitative Approach* (New York: Kluwer Academic/Plenum)

Plonsey R and Collin R E 1961 *Principles and Applications of Electromagnetic Fields* (New York: McGraw-Hill)

Plonsey R and Heppner D B 1967 Considerations of quasi-stationarity in electrophysiological systems *Bull. Math. Biophys.* **29** 657–64

Stinstra J G and Peters M J 1998 The volume conductor may act as a temporal filter on the ECG and EEG *Med. Biol. Eng. Comput.* **36** 711–6